

Simulation Study of Ballooning Modes in the Large Helical Device

Yasushi TODO, Noriyoshi NAKAJIMA, Masahiko SATO and Hideaki MIURA

National Institute for Fusion Science, 322-6 Oroshi-cho, Toki 509-5292, Japan

(Received 24 December 2009 / Accepted 1 March 2010)

The magnetohydrodynamic (MHD) simulation code MHD Infrastructure for Plasma Simulation (MIPS) was benchmarked on ballooning instability in the Large Helical Device (LHD) plasma. The results were compared to the results of linear analysis by using the CAS3D code. Both the linear growth rates and the spatial profiles were found to be in good agreement. An extended MHD model with finite ion Larmor radius effects was implemented into the MIPS code. Ballooning instabilities were investigated using the extended MHD model, and the results were compared with those using the MHD model. Ion diamagnetic drift was found to reduce the growth rate of the short-wavelength modes; hence, modes with a diamagnetic drift frequency comparable to the ideal MHD growth rate are the most unstable. The most unstable toroidal mode number of ballooning instability in the LHD is reduced to $|n| \leq 5$ for hydrogen plasma with ion number density $n_i \leq 10^{19} \text{ m}^{-3}$.

© 2010 The Japan Society of Plasma Science and Nuclear Fusion Research

Keywords: ballooning modes, MHD, ion diamagnetic drift, Large Helical Device, computer simulation

DOI: 10.1585/pfr.5.S2062

1. Introduction

Magnetohydrodynamics (MHD) provides a basic model of the macroscopic behaviors of plasmas. The MHD model is generally used for theoretical and computational analyses of fusion plasmas. The MHD simulation code, MHD Infrastructure for Plasma Simulation (MIPS) can be applied to toroidal plasmas and used as a basis for extended-MHD simulations. The MIPS code is parallelized using the Message-Passing-Interface (MPI). In this paper, we report on the benchmark of the MIPS code for ballooning instability in the Large Helical Device (LHD).

Recently, we have implemented an extended-MHD model presented by Hazeltine and Meiss [1] into the MIPS code. MHD simulation of LHD plasma revealed that the ballooning modes with high toroidal mode number are unstable and lead to significant flattening of the pressure profile [2]. The ballooning modes with higher mode numbers are known to be more unstable. It is interesting to investigate how the ballooning modes are affected by the ion finite Larmor radius effects, which are retained in the Hazeltine-Meiss model. We compare the results with the MHD results.

2. Benchmark of MIPS Code

The MIPS code uses cylindrical coordinates (R, φ, z) and solves the MHD equations described below.

$$\frac{\partial \rho}{\partial t} = -\nabla \cdot (\rho \mathbf{v}), \quad (1)$$

$$\begin{aligned} \rho \frac{\partial}{\partial t} \mathbf{v} = & -\rho \mathbf{w} \times \mathbf{v} - \rho \nabla \left(\frac{v^2}{2} \right) - \nabla p + \mathbf{j} \times \mathbf{B} \\ & + \frac{4}{3} \nabla [v \rho (\nabla \cdot \mathbf{v})] - \nabla \times [v \rho \mathbf{w}], \end{aligned} \quad (2)$$

author's e-mail: todo@nifs.ac.jp

$$\frac{\partial \mathbf{B}}{\partial t} = -\nabla \times \mathbf{E}, \quad (3)$$

$$\begin{aligned} \frac{\partial p}{\partial t} = & -\nabla \cdot (p \mathbf{v}) - (\gamma - 1) p \nabla \cdot \mathbf{v} \\ & + (\gamma - 1) \left[v \rho w^2 + \frac{4}{3} v \rho (\nabla \cdot \mathbf{v})^2 + \eta \mathbf{j} \cdot (\mathbf{j} - \mathbf{j}_{\text{eq}}) \right], \end{aligned} \quad (4)$$

$$\mathbf{E} = -\mathbf{v} \times \mathbf{B} + \eta (\mathbf{j} - \mathbf{j}_{\text{eq}}), \quad (5)$$

$$\mathbf{j} = \frac{1}{\mu_0} \nabla \times \mathbf{B}, \quad (6)$$

$$\mathbf{w} = \nabla \times \mathbf{v}. \quad (7)$$

Here, μ_0 is the vacuum magnetic permeability, γ is the adiabatic constant, and \mathbf{j}_{eq} is the equilibrium current density that is considered to make the MHD equilibrium consistent with the finite resistivity. The spatial derivatives are calculated by a finite difference method of fourth-order accuracy. The fourth-order Runge-Kutta method is used for the time integration.

The MIPS code was benchmarked on the ballooning modes in the LHD plasma. The initial equilibrium was constructed using the HINT code [3] for the inward-shifted magnetic configuration with $R_{\text{ax}} = 3.6 \text{ m}$ and the free net toroidal current. The equilibrium was investigated in Ref. [2]; the spatial profiles of the beta value and rotational transform are shown in Fig. 1. A uniform density profile is assumed. A Boozer coordinate system of the equilibrium was constructed for the spectral analysis of the simulation results. Viscosity and resistivity values of $\nu = \eta/\mu_0 = 10^{-6} v_A R_{\text{axis}}$ are chosen for numerical stability, where v_A and $R_{\text{axis}} = 3.78 \text{ m}$ are the Alfvén velocity at the magnetic axis and the major radius of the magnetic axis, respectively. The numbers of grid points are (128, 640, 128). The computational performance of the MIPS code

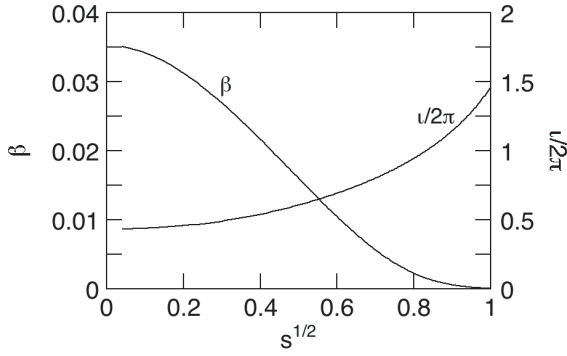


Fig. 1 Spatial profiles of the beta value and rotational transform of the initial equilibrium.

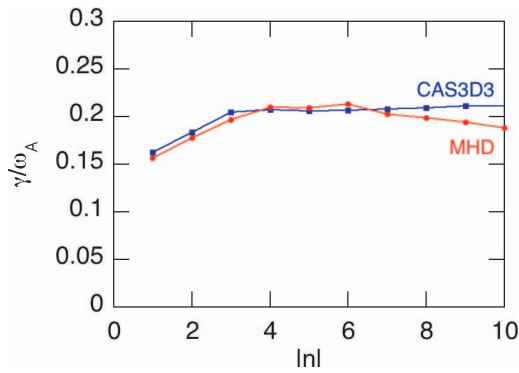


Fig. 2 Comparison of ballooning mode growth rate calculated using MIPS (red circles) and CAS3D (blue squares) for different toroidal mode numbers.

by using 32 cores of the POWER6 processor (5.0 GHz) of the Plasma Simulator (HITACHI SR16000) is 82 Gflops. This is 13% of the theoretical peak performance.

The results of the MIPS code were compared with those of the MHD linear analysis code CAS3D [4]. The linear growth rates of the ballooning modes in the two results are compared in Fig. 2. The growth rate is normalized by the Alfvén frequency $\omega_A = v_A/R_{axis}$. We observe good agreement for low toroidal modes ($|n| \leq 7$), whereas for $|n| \geq 8$, the MIPS simulation shows lower growth rates than the CAS3D analysis. The numbers of poloidal grid points used in the MIPS code may not be sufficient to resolve the spatial profiles of the higher- n ballooning modes. The finite viscosity and resistivity assumed in the simulation is another factor in the lower growth rate for higher- n modes, because the viscous and resistive terms are second-order spatial derivatives. The radial velocity profiles of the ballooning mode with $n = -4$ are compared in Fig. 3. Good agreement appears between the MIPS simulation and the CAS3D analysis. Thus, we can conclude that the MIPS code is a useful tool for simulation studies of MHD instabilities in the LHD.

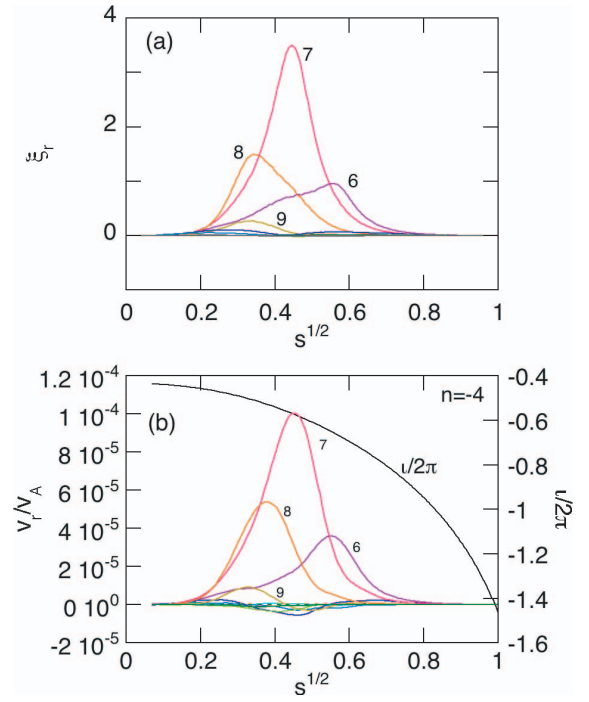


Fig. 3 Comparison of the radial velocity profiles of the $n = -4$ ballooning mode in (a) the CAS3D analysis and (b) the MIPS simulation. Horizontal axis represents the square root of the normalized toroidal magnetic flux. Poloidal mode numbers are indicated in the figure.

3. Simulation by Using the Hazeltine-Meiss Model

The extended-MHD model presented by Hazeltine and Meiss [1] was implemented in the MIPS code. Ion finite Larmor radius effects can be investigated using this model. The electron and ion pressures are assumed to be equal. The Hazeltine-Meiss model is given by the following equations.

$$\frac{\partial \rho}{\partial t} = -\nabla \cdot (\rho \mathbf{v}), \quad (8)$$

$$\begin{aligned} \rho \frac{\partial}{\partial t} \mathbf{v}_{\text{MHD}} = & -\rho \mathbf{v} \cdot \nabla \mathbf{v}_{\text{MHD}} + \rho \mathbf{v}_{\text{pi}} \cdot \nabla (v_{\parallel} \mathbf{b}) - \nabla p \\ & + \mathbf{j} \times \mathbf{B} + \frac{4}{3} \nabla [v \rho (\nabla \cdot \mathbf{v}_{\text{MHD}})] \\ & - \nabla \times [v \rho \mathbf{w}], \end{aligned} \quad (9)$$

$$\frac{\partial \mathbf{B}}{\partial t} = -\nabla \times \mathbf{E}, \quad (10)$$

$$\begin{aligned} \frac{\partial p}{\partial t} = & -\nabla \cdot (p \mathbf{v}_{\text{MHD}}) - (\gamma - 1) p \nabla \cdot \mathbf{v}_{\text{MHD}} \\ & + (\gamma - 1) \left[v \rho w^2 + \frac{4}{3} v \rho (\nabla \cdot \mathbf{v}_{\text{MHD}})^2 + j_{\parallel} E_{\parallel} \right], \end{aligned} \quad (11)$$

$$v_{\parallel} = \mathbf{v}_{\text{MHD}} \cdot \mathbf{b}, \quad (12)$$

$$\mathbf{v}_E = \mathbf{v}_{\text{MHD}} - v_{\parallel} \mathbf{b}, \quad (13)$$

$$\mathbf{w} = \nabla \times \mathbf{v}_{\text{MHD}}, \quad (14)$$

$$\mathbf{v}_{\text{pi}} = \frac{Am_H}{2Ze\rho B^2} \mathbf{B} \times \nabla p, \quad (15)$$

$$\mathbf{j} = \frac{1}{\mu_0} \nabla \times \mathbf{B}, \quad (16)$$

$$\mathbf{v} = \mathbf{v}_{\text{MHD}} + \mathbf{v}_{\text{pi}} + \frac{Am_{\text{H}}}{Ze\rho} \mathbf{j}_{\perp}, \quad (17)$$

$$\mathbf{E}_{\perp} = -\mathbf{v}_E \times \mathbf{B}, \quad (18)$$

$$\mathbf{E}_{\parallel} = -\frac{Am_{\text{H}}}{2e\rho} \nabla_{\parallel} P + \eta(\mathbf{j}_{\parallel} - \mathbf{j}_{\parallel \text{eq}}). \quad (19)$$

Here, m_{H} , A , and Z are the hydrogen mass, ion atomic number, and ion charge numbers, respectively.

Equations (8)-(19) resemble the MHD equations. However, ion finite Larmor radius effects are retained in the Hazeltine-Meiss model. The dispersion relation of the kinetic Alfvén wave was reproduced by a numerical code that implements Eqs. (8)-(19) [5]. In this model, the time derivative in the momentum equation [Eq. (9)] appears for the MHD velocity and not for the total velocity \mathbf{v} given by Eq. (17). The total velocity contains the perpendicular current density term in Eq. (17), and the perpendicular current density can be expressed using the time derivative of the MHD velocity, as seen in Eq. (9). Thus, the time derivative of the total velocity contains the second-order time derivative of the MHD velocity. This would make the equation system more complicated and difficult to simulate. On the other hand, the momentum equation [Eq. (9)] describes the evolution of the MHD velocity. This makes the simulation relatively easy to conduct. In this paper, two differences from the original Hazeltine-Meiss model appear in the equation system. The pressure evolution equation [Eq. (11)] differs slightly from that in Ref. [1], because the MHD velocity \mathbf{v}_{MHD} in this paper is simply related to the $E \times B$ velocity and the parallel velocity by Eqs. (12) and (13), whereas in Ref. [1], the MHD velocity is defined by $\mathbf{v}_{\text{MHD}} = \mathbf{v} - \mathbf{v}_{\text{pi}}$. With the original definition we found that the equation system is numerically unstable, so we used a different \mathbf{v}_{MHD} in Eq. (11). The MHD velocity also appears in Eq. (9). However, Eq. (9) is identical to its counterpart in Ref. [1] if we neglect the viscous terms, which are not included in the original equation system.

The ballooning mode growth rate and real frequency in LHD plasma investigated using the MHD and Hazeltine-Meiss models are shown in Fig. 4. Two different hydrogen plasmas were investigated using the Hazeltine-Meiss model for different ion number densities $n_i = 1.6 \times 10^{19} \text{ m}^{-3}$ and $n_i = 4 \times 10^{18} \text{ m}^{-3}$ with $A = 1$ and $Z = 1$. The Hazeltine-Meiss model shows a reduced growth rate and finite frequency. The difference from the MHD results is greater for the lower density case ($n_i = 4 \times 10^{18} \text{ m}^{-3}$) and higher mode numbers. In this case, the most unstable mode is $n = -3$ and the growth rate of the middle- and higher- n ($|n| \geq 4$) modes is significantly reduced. For the moderate-density case ($n_i = 1.6 \times 10^{19} \text{ m}^{-3}$), the most unstable mode is $n = -5$ and the growth rate of the higher- n ($|n| \geq 6$) modes are more reduced than the lower- n modes. We can say that the most unstable toroidal mode number of the ballooning instability in LHD hydrogen plasma is reduced using the Hazeltine-Meiss model to $|n| \leq 5$ for ion

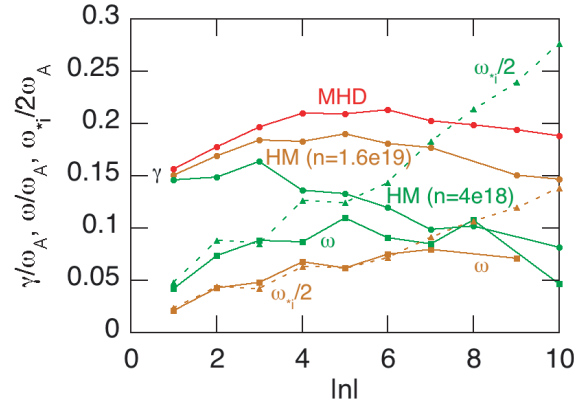


Fig. 4 Growth rate and frequency of ballooning instabilities in the LHD vs. toroidal mode number. MHD model results are shown in red; Hazeltine-Meiss model results for hydrogen plasma are shown in brown ($n_i = 1.6 \times 10^{19} \text{ m}^{-3}$) and green ($n_i = 4 \times 10^{18} \text{ m}^{-3}$). Dashed curves represent $\omega_{*i}/2$.

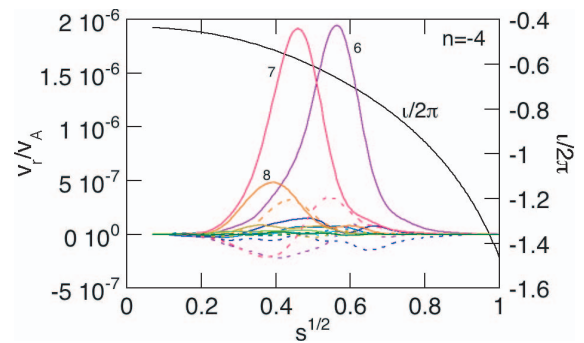


Fig. 5 Radial velocity profile of the $n = -4$ ballooning mode in the LHD simulated using the Hazeltine-Meiss model for hydrogen plasma with number density $n_i = 4 \times 10^{18} \text{ m}^{-3}$. Solid (dashed) curves represent cosine (sine) components of the harmonics. Horizontal axis represents the square root of the normalized toroidal magnetic flux.

number density $n_i \leq 10^{19} \text{ m}^{-3}$.

The spatial profile of the ballooning mode with toroidal mode number $n = -4$ for $n_i = 4 \times 10^{18} \text{ m}^{-3}$ is shown in Fig. 5. The $m/n = 6/-4$ harmonic is greater than that in the MHD case, as shown in Fig. 3. In Fig. 5, the sine harmonics appear in addition to the cosine harmonics, whereas the sine harmonics are negligibly small in Fig. 3. In both figures, we chose the phase of the harmonics to maximize the cosine component of the dominant harmonics. The self-adjointness of the ideal MHD model yields only the cosine harmonics for the chosen phase. Thus, the appearance of the sine harmonics in Fig. 5 indicates that self-adjointness is broken in the Hazeltine-Meiss model. This is also indicated by the combination of finite growth rate and finite frequency corresponding to a complex eigenvalue.

4. Discussion

Let us consider what causes the differences from the MHD model. Ion diamagnetic drift has been predicted to have a stabilizing effect on MHD instability and give it a finite frequency of one-half the ion diamagnetic drift frequency (ω_{*i}) [6]. The stabilizing effect is stronger for higher ω_{*i} , and the instability is stabilized when ω_{*i} is two times the ideal MHD growth rate. In Fig. 4, we show $\omega_{*i}/2$ defined with the dominant poloidal mode number at the peak location of the spatial profile. The real frequency of the instability agrees well with the theoretically predicted $\omega_{*i}/2$ for lower toroidal mode numbers for which ω_{*i} is smaller than the ideal MHD growth rate. Because the theory given in Ref. [6] is based on a perturbative approach in which the spatial profile of the instability is assumed to be the same as that of the ideal MHD instability, it is not applicable to the values of ω_{*i} equal to or higher than the ideal MHD growth rate, where the spatial profile deviates from the ideal MHD profile, as shown in Figs. 3 and 5. The toroidal coupling induced by the diamagnetic drift may lead to a relatively large $m/n = 6/-4$ harmonic shown in Fig. 5. The results shown in Fig. 4 indicate that ion diamagnetic drift effects reduce the growth rate of the short-wavelength modes, so modes with a diamagnetic drift frequency comparable to the ideal MHD growth rate ($\omega_{*i} \sim \gamma_{\text{MHD}}$) are most unstable.

The diamagnetic drift frequency is estimated by the following equation, with the definition of the ion diamagnetic velocity defined by Eq. (15),

$$\frac{\omega_{*i}}{\omega_A} \equiv \frac{\mathbf{v}_{pi} \cdot \nabla}{\omega_A} \sim \frac{m\beta}{4} \left(\frac{R}{r} \right) \left(\frac{v_A/\Omega_i}{L} \right), \quad (20)$$

where L , m , and Ω_i are the pressure scale length, poloidal mode number of the instability, and ion gyro frequency, respectively. It is interesting that the scale length v_A/Ω_i is identical to the ion skin length c/ω_{pi} , where ω_{pi} is the ion plasma frequency. The ion skin length depends on the ion mass, charge, and number density. Thus, Eq. (20) can be rewritten as

$$\frac{\omega_{*i}}{\omega_A} \sim 1.8 \times 10^{-2} \beta mA^{1/2} Z^{-1} \times \left[\frac{n_i}{10^{19} \text{ m}^{-3}} \right]^{-1/2} \left[\frac{a}{1 \text{ m}} \right]^{-1} \left(\frac{a^2}{rL} \right) \left(\frac{R}{a} \right), \quad (21)$$

where n_i is the ion number density of the plasma and a is the plasma minor radius. For LHD plasmas with $a = 0.6 \text{ m}$,

$R/a = 6$, and $a^2/rL = 6$, Eq. (21) is reduced to

$$\frac{\omega_{*i}}{\omega_A} \sim \beta mA^{1/2} Z^{-1} \left[\frac{n_i}{10^{19} \text{ m}^{-3}} \right]^{-1/2}. \quad (22)$$

For a beta of 2%, a number density of 10^{19} m^{-3} , and a poloidal mode number $m \sim 10$, Eq. (22) yields a value of 0.2. This is a level comparable to the ballooning mode growth rate shown in Fig. 2. This indicates that ion diamagnetic drift is important in reducing the growth rate for higher mode numbers.

5. Conclusion

We have found a good agreement between simulation results by using the MHD simulation code MIPS and linear analysis results by using the CAS3D code for ballooning instability in LHD plasma. The MIPS code is a useful tool for investigating MHD phenomena in toroidal plasmas. Furthermore, we have implemented the extended-MHD model presented by Hazeltine and Meiss, which retains ion finite Larmor radius effects, in the MIPS code. Ion diamagnetic drift effects were found to reduce the growth rate of the short-wavelength modes; hence, modes with a diamagnetic drift frequency comparable to the ideal MHD growth rate are the most unstable. The most unstable toroidal mode number of the ballooning instability is reduced to $|n| \leq 5$ for hydrogen plasma with ion number density $n_i \leq 10^{19} \text{ m}^{-3}$.

Acknowledgments

Numerical computations were performed at the Plasma Simulator (HITACHI SR16000) of the National Institute for Fusion Science. This study was supported by the NIFS Collaborative Research Program (NIFS09KTAL021) and a Grant-in-Aid for Scientific Research from the Japan Society for the Promotion of Science (No. 20340165).

- [1] R. D. Hazeltine and J. D. Meiss, *Plasma Confinement* (Addison-Wesley, Redwood City) p.222 (1992).
- [2] H. Miura and N. Nakajima, *Nucl. Fusion* **50**, 054006 (2010).
- [3] K. Harafuji, T. Hayashi and T. Sato, *J. Comput. Phys.* **81**, 169 (1989).
- [4] C. Nührenberg, *Phys. Plasmas* **6**, 137 (1999).
- [5] Y. Todo, *J. Plasma Phys.* **72**, 817 (2006).
- [6] N. Nakajima, S. R. Hudson, C. C. Hegna and Y. Nakamura, *Nucl. Fusion* **46**, 177 (2006).